PHILOSOPHICAL MAGAZINE A, 1999, VOL. 79, NO. 10, 2339–2358

Introduction of a scalable three-dimensional cellular automaton with a probabilistic switching rule for the discrete mesoscale simulation of recrystallization phenomena

DIERK RAABE†

Institut für Metallkunde und Metallphysik, Rheinisch–Westfälische Technische Hochschule Aachen, Kopernikusstr.14, 52056 Aachen, Germany

[*Received 13 July 1998 and accepted in revised form 10 November 1998*]

ABSTRACT

The paper introduces a scalable three-dimensional (3D) kinetic cellular automaton model with a probabilistic switching rule for the spatial and crystallographic prediction of mesoscale transformation phenomena that involve orientational field variables and the motion of sharp interfaces, such as encountered in the field of recrystallization. The automaton is discrete in time, physical space and Euler orientation space. It is defined on a regular 3D cubic lattice considering the first-, second- and third-neighbour shells for the calculation of the local driving forces. The kinetic transformation rule is formulated as a probabilistic analogue of the classical linearized symmetric Turnbull rate equation for grain-boundary segment motion. It is used to calculate the switching probability of each grid point as a function of its previous state and the state of the neighbouring grid points. The actual decision about a switching event is made by evaluating the local switching probability using a Monte Carlo step. The transformation rule is scaled by the ratio of the local to the maximum possible grain boundary mobility, the local crystallographic texture, and the ratio of the local to the maximum occurring driving force. The time step of the simulation is determined by the maximum occurring driving force, by the maximum occurring grain boundary mobility and by the spacing of the grid points. The use of realistic or even experimental input data for the boundaries allows one to make predictions on a real time and space scale. The transformation rule is scalable to any mesh size and to any spectrum of boundary mobility and energy data. The state update of all grid points is made in synchrony. The model predicts the kinetics, the evolution of the grain size and topology, and the evolution of the crystallographic texture during recrystallization.

§1. BASIC MOTIVATION AND JUSTIFICATION OF A NEW MODEL

Three-dimensional (3D) time and space discretized simulations of materials microstructures which track kinetics and energies in a local fashion are of interest for two reasons. First, from a fundamental point of view it is desirable to understand better the dynamics and the topology of microstructures that arise from the interaction of large numbers of lattice defects which are characterized by a wide spectrum of intrinsic properties in spatially heterogeneous materials. For instance, in the field

† Correspondence to: Dierk Raabe, Luchweg 10, D-14621 Schönwalde, Germany; email, dierk.raabe@t-online.de.

Philosophical Magazine A ISSN 0141–8610 print/ISSN 1460-6992 online
http://www.tandf.co.uk/JNLS/phm.htm
http://www.taylorandfrancis.com/JNLS/phm.htm

of recrystallization the influence of local grain boundary characteristics (mobility and energy), local driving forces and local crystallographic textures on the final microstructure is of particular interest. Second, from a practical point of view it is necessary to predict microstructure parameters such as grain size or texture which determine the mechanical and physical properties of real materials subjected to industrial processes on a phenomenological although sound physical basis.

A number of excellent models for discretely simulating recrystallization and grain growth phenomena have been suggested. They can be grouped as multistate kinetic Potts Monte Carlo models (Srolovitz 1986, Anderson and Rollett 1990, Holm *et al.* 1996), deterministic cellular automata (Hesselbarth and Göbel 1991, Pezzee and Dunand 1994, Marx *et al.* 1996, 1998), topological boundary dynamics and front-tracking models (Frost and Thompson 1987, Frost *et al.* 1990, Humphreys 1992, 1997, Fradkov *et al.* 1994, Svoboda 1996), component models (Juul Jensen 1992, 1997) and Ginzburg-Landau-type phase field kinetic models (Chen 1995, Fan *et al.* 1997).

Complementary to these approaches, this paper introduces a new scalable kinetic probabilistic cellular automaton method with the aim of combining the computational simplicity and scalability of a switching model with the physical stringency of a boundary dynamics model (Raabe 1998a,b). Its objective lies in providing a numerically efficient and at the same time phenomenologically sound method of discretely simulating recrystallization phenomena in three dimensions. As far as computational aspects are concerned, the approach is designed to minimize the calculation time and to reduce the code complexity in terms of storage and algorithm. As far as microstructure physics is concerned, it is designed to provide kinetics, texture and microstructure on a real space and time scale on the basis of microtexture, grain-boundary characteristics and local driving forces. The possible incorporation of realistic values particularly for grain-boundary energies and mobilities deserves particular attention since such experimental data are increasingly available (Gottstein *et al.* 1995, Shvindlerman *et al.* 1995, Adams *et al.* 1998, Molodov *et al.* 1998) enabling one to make *quantitative* predictions. This paper gives an introduction to the method and presents applications in the field of primary static recrystallization.

§ 2. Basic structure of the probabilistic cellular automaton

The model is designed as a 3D cellular automaton with a probabilistic transformation rule. This means that the switch of the state of a grid point is not performed in a deterministic fashion, say, like in a Pascal triangle, but with a certain probability. The basic transformation (switching) rule of the automaton consists of a probabilistic analogue of the linearized symmetric rate equation for thermally activated grain-boundary segment motion under the influence of free energy gradients as introduced by Turnbull (1951). According to this rate equation the local switching probability is for each grid point calculated using the local and maximum driving force, the local texture, and the local and maximum boundary mobility. This first step of the switching algorithm is strictly deterministic. The use of realistic boundary mobility and energy data introduces a real space and time scale into the model. After having calculated the switching probability the actual decision about the switch is made using a Monte Carlo step. This second step of the switching algorithm is probabilistic. It represents an importance or weighted sampling integration of the probability function that is given by the Turnbull equation. Since all possible switching probabilities that occur in one simulation are normalized with respect to

the fastest moving boundary in the system, a broad variety of mobilities and energies can be considered simultaneously.

The Turnbull equation is used in a scaled form so that an increase in the jump width leads to a corresponding decrease in the attack frequency. Therefore, the length scale of the grid (which equals the size of a lattice cell, mesh size or jump width) can be freely chosen in accord with any characteristic initial microstructural length scale without spoiling the overall time scale. All possible cell switches are considered in each time step. The state update is for all successfully switched cells made in synchrony once during each simulation time step.

The material properties are regarded as continuum field quantities. To apply the switching algorithms that characterize cellular automata the physical space (the sample) must be discretized into a regular array of equally shaped cells (figure 1 (*a*)). The time t and space $\mathbf{x} = (x_1, x_2, x_3)$ act as independent variables. The crystal grain orientation $\mathbf{g} = \mathbf{g}(\varphi_1, \phi, \varphi_2)$, where φ_1, ϕ and φ_2 are the three Euler angles, and mechanical, interface or electromagnetic contributions to the Gibbs free energy G_t are dependent variables. The automaton is defined on a spatially discrete 3D cubic lattice considering the first, second- and third-neighbour shells. Each discrete lattice cell is then characterized by an orientation and a value for the stored free energy, for example by the deformation energy in recrystallization simulations. Grains or subgrains are mapped as regions of identical crystal orientation (figure 1 (*b*)). The driving force may vary inside grains and subgrains. The boundary mobility m is a function of the crystal misorientation $\Delta\mathbf{g}$ (e.g. expressed in terms of rotation angle and rotation axis) and the boundary plane inclination $\mathbf{n}$. Both quantities are derived dependent variables. Simulations require the incorporation of experimental or theoretical data for grain-boundary mobilities and energies as functions of their crystallographic misorientation.

The new approach allows one to conduct fast discrete 3D simulations of the evolution of grain microstructures in physical and crystallographic orientation space on a realistic time and space scale. It considers the initial microstructure including crystallographic textures, grain-boundary characteristics (energy and mobility) and driving forces. The following sections provide a more detailed derivation of the governing rate equation and its probabilistic analogue which serves as local transformation rule, of the normalization and of the switching scheme (Monte Carlo step). Finally, some kinetic and topological results of recrystallization simulations will be discussed and compared with analytical predictions.

§ 3. Turnbull's rate equation of boundary motion as a starting point for deriving the transformation rule

According to Turnbull (1951) a phenomenological symmetric rate equation, which describes grain-boundary motion in terms of isotropic single-atom diffusion processes perpendicular through a homogeneous planar grain boundary segment under the influence of free energy gradients, can be written

$$\begin{aligned}\dot{\mathbf{x}} &= \mathbf{n}\nu_D\lambda_{gb}c\left[\exp\left(-\frac{(\Delta G+\Delta G_t)/2}{k_BT}\right)-\exp\left(-\frac{(\Delta G-\Delta G_t)/2}{k_BT}\right)\right]\\ &= \mathbf{n}\nu_D\lambda_{gb}\exp\left(-\frac{\Delta H^f-\Delta S^f T}{k_BT}\right)\left[\exp\left(-\frac{\Delta H^m-T\Delta S^m-(p\Omega)/2}{k_BT}\right)\right.\\ &\quad\left.-\exp\left(-\frac{\Delta H^m-T\Delta S^m+(p\Omega)/2}{k_BT}\right)\right],\end{aligned}\tag{1}$$

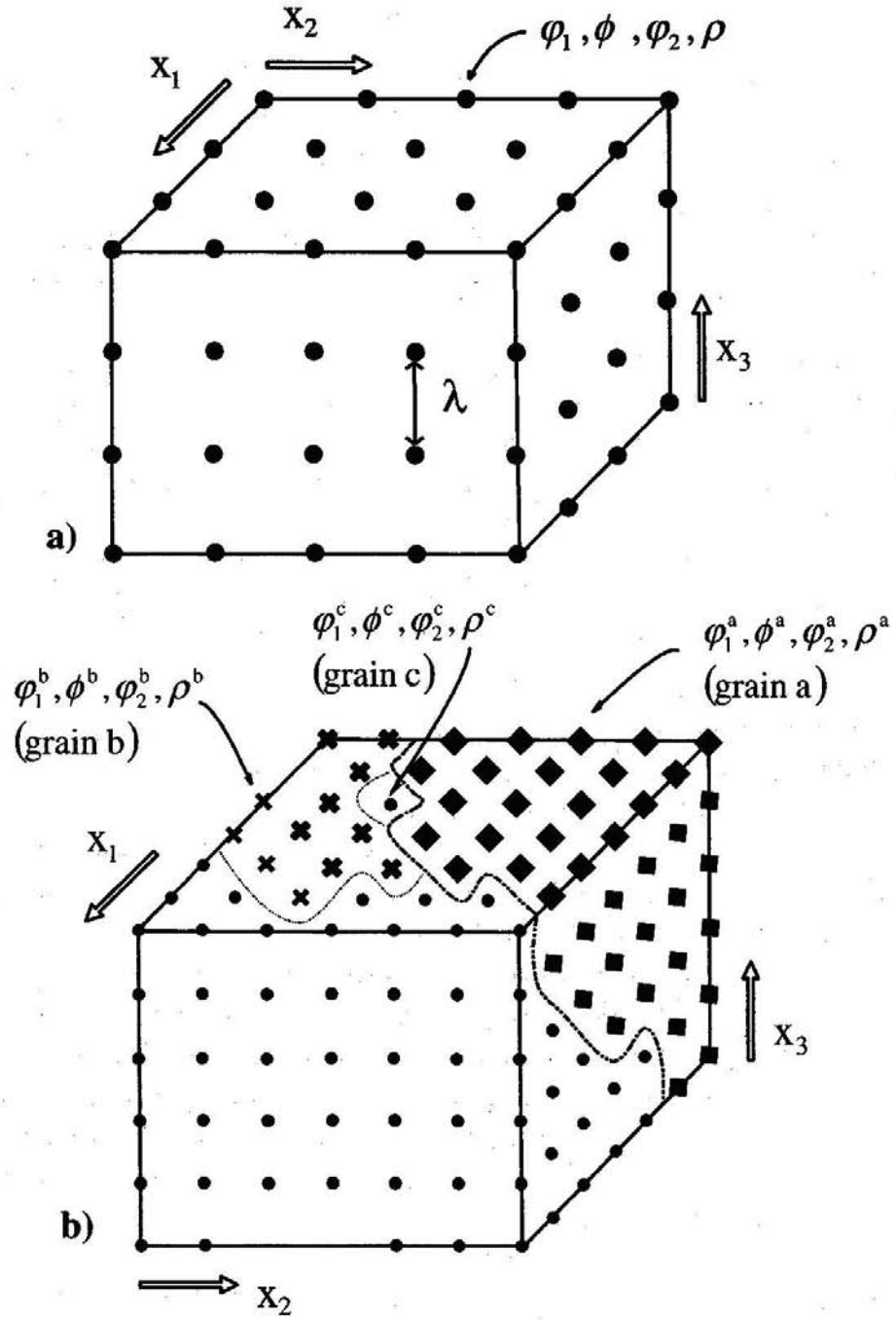

Figure 1. (*a*) Basic set-up of the simulation grid. The sample is discretized into a regular array of equally shaped cells. Time t and space $\mathbf{x} = (x_1, x_2, x_3)$ are independent variables. Each cell is characterized by its crystal orientation $\mathbf{g} = \mathbf{g}(\varphi_1, \phi, \varphi_2)$, where φ_1, ϕ and φ_2 are the Euler angles, and a stored energy value (for recrystallization simulations). ρ indicates the stored dislocation density. The automaton is defined on a 3D cubic lattice considering the first-, second- and third-neighbour shells. (*b*) Grains or subgrains are mapped as regions of cells which have identical crystal orientations. The driving force may vary inside grains.

where $\dot{\mathbf{x}}$ is the interface velocity, ν_D the Debye frequency, λ_{gb} the jump width through the interface, c the intrinsic concentration of in-plane self diffusion carrier defects (e.g. grain-boundary vacancies or shuffle sources), $\mathbf{n}$ the normal of the grain-boundary segment, ΔG the Gibbs enthalpy of motion through in the interface, ΔG_t the Gibbs enthalpy associated with the transformation, p the negative gradient in Gibbs enthalpy across the interface (driving force), Ω the atomic volume, ΔS^f the entropy of formation, ΔH^f the enthalpy of formation, ΔS^m the entropy of motion, ΔH^m the enthalpy of motion, k_B the Boltzmann constant and T the absolute

temperature. The atomic volume is of the order of b^3, where b is the magnitude of the Burgers vector. Bold symbols indicate vector quantities. The Debye frequency is of the order of 10^{13}–$10^{14}\,s^{-1}$ and the jump width is of the order of the magnitude of the Burgers vector. Summarizing these terms leads to

$$\dot{\mathbf{x}} = \mathbf{n}\nu_D b \exp\left(-\frac{\Delta S^f + \Delta S^m}{k_B}\right)\sinh\left(\frac{p\Omega}{k_B T}\right)\exp\left(-\frac{\Delta H^f + \Delta H^m}{k_B T}\right)$$
$$\approx \mathbf{n}\nu_D b \exp\left(-\frac{\Delta S^f + \Delta S^m}{k_B}\right)\frac{p\Omega}{k_B T}\exp\left(-\frac{\Delta H^f + \Delta H^m}{k_B T}\right), \tag{2}$$

which reproduces the well known phenomenological Turnbull expression

$$\dot{\mathbf{x}} = \mathbf{n}mp = \mathbf{n}m_0 \exp\left(-\frac{Q_{gb}}{k_B T}\right)p, \tag{3}$$

where m is the mobility and Q_{gb} the activation energy of boundary motion. Equations (1)–(3) provide a well known phenomenological kinetic picture, where the atomistic processes associated with grain-boundary motion are statistically described in terms of $m_0 = m_0(\Delta\mathbf{g}, \mathbf{n})$ and $Q_{gb} = Q_{gb}(\Delta\mathbf{g}, \mathbf{n})$.

§4. Probabilistic analogue of Turnbull's rate equation

This section is concerned with the replacement of the deterministic rate equation of boundary segment motion, equation (3), by a probabilistic analogue which can be used for the calculation of switching *probabilities*. For this purpose, equation (3) can be separated into a deterministic part, $\dot{\mathbf{x}}_0$, which depends weakly on temperature, and a probabilistic part, w, which depends strongly on temperature:

$$\dot{\mathbf{x}} = \dot{\mathbf{x}}_0 w = \mathbf{n}\frac{k_B T m_0}{\Omega}\frac{p\Omega}{k_B T}\exp\left(-\frac{Q_{gb}}{k_B T}\right), \tag{4}$$

where

$$\dot{\mathbf{x}}_0 = \mathbf{n}\frac{k_B T m_0}{\Omega}$$

and

$$w = \frac{p\Omega}{k_B T}\exp\left(-\frac{Q_{gb}}{k_B T}\right).$$

It is worth noting that the probability factor w simply represents the product of the linearized part $(p\Omega)/(k_B T)$ and the non-linearized part $\exp(-Q_{gb}/(k_B T))$ of the original Boltzmann terms, equations (1) and (2). Figure 2 shows the non-normalized probability factor as a function of absolute temperature and driving force for an average aluminium large-angle grain-boundary with an activation energy of the mobility of $Q_{gb} = 1\,eV$ (equation (4)). The normalization procedure which shifts the switching probabilities to larger values is explained in §6.

According to equation (4), non-vanishing switching probabilities can occur for lattice cells which reveal neighbouring cells with different crystallographic orientations and a driving force which points in their direction. The local value of the switching probability depends on the crystallographic character of the boundary segment between such unlike cells.

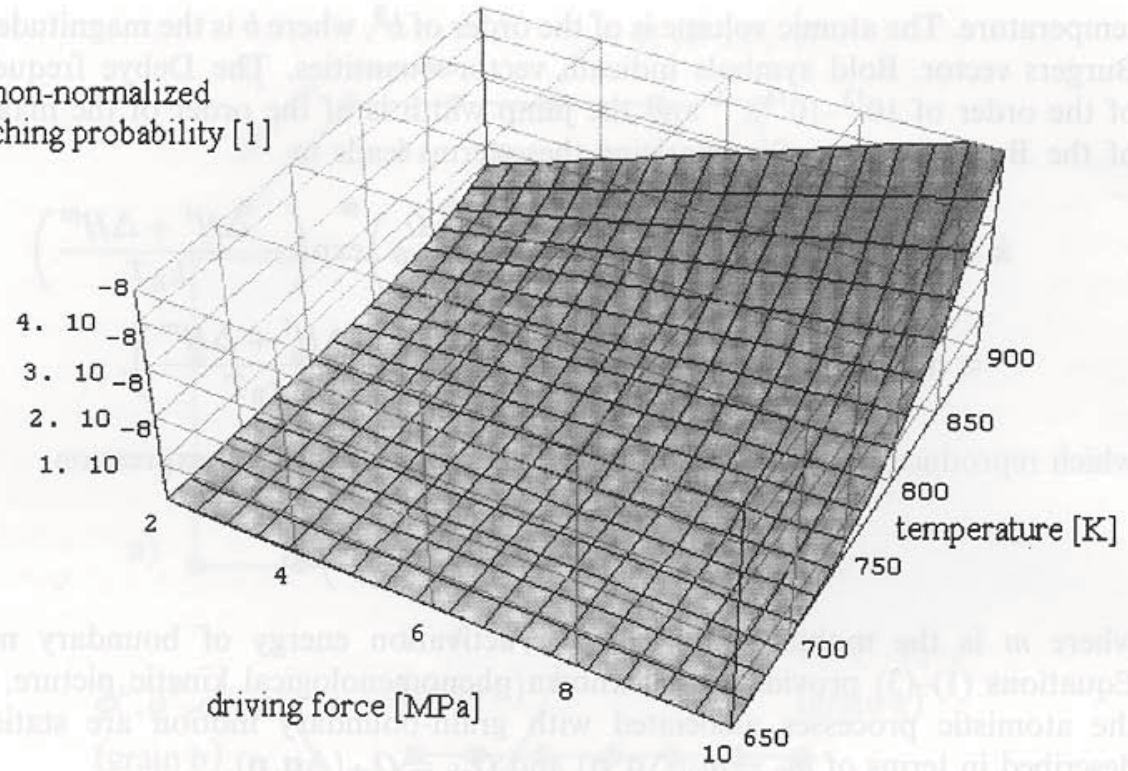

Figure 2. Plot of the non-normalized probability factor $(p\Omega)/(k_B T)\exp(-Q_{gb}/(k_B T))$ as a function of absolute temperature and driving force for an average aluminium large-angle grain boundary with an activation energy of the mobility of $Q_{gb} = 1\,\text{eV}$. The probability factor represents the linearized and the nonlinearized part of the Boltzmann terms in equations (1) and (2).

§ 5. Reformulation of the switching probability in accord with the length scale and eigenfrequency of the simulation grid

The validity of the Turnbull rate equation for grain boundary motion is not confined to the atomic scale but strictly fulfilled at any scale. This can be demonstrated by the following estimation: The displacement frequency† Γ normal to a boundary segment with given Q_{gb} is given by

$$\Gamma = \frac{m_0 p}{\lambda} \exp\left(-\frac{Q_{gb}}{k_B T}\right), \tag{5}$$

where λ is the jump width. The number of atoms displaced per second then is $N\Gamma$ when N is the number of atoms in the crystal plane bordering on the boundary. The interface displacement per second then amounts to $N\Gamma/N$. Since the jump width is determined by the magnitude of the velocity, that is $\dot{x} = \Gamma\lambda$, the displacement rate of the grain boundary segment depends only on macroscopic phenomenological parameters.

The cellular automaton simulations are conducted on a spatial cubic grid with an arbitrarily chosen mesh size λ_m. In a mesoscopic simulation the value of λ_m will usually be much larger than the atomic spacing b. If a moving boundary segment sweeps a cell, the grain thus grows (or shrinks) by λ_m^3 rather than b^3. Since the net

† The displacement frequency Γ must not be confused with the attack frequency ν. While the attack frequency gives the number of all *trial* jumps per time interval, the displacement frequency gives the number of all *successful* attempts per time interval.

velocity of a boundary segment must be independent of the imposed value of λ_m, an increase in the jump width must lead to a corresponding decrease in the grid attack frequency and vice versa. In other words, to obtain a scale-independent net velocity of the grain boundary, the mesoscopic grid frequency must be chosen in such a way as to ensure that the attempted switch of a cell of length λ_m occurs with a frequency much below the atomic attack frequency which attempts to switch a cell of length b. The prescribed scaling length λ_m turns equation (4) into

$$\dot{\mathbf{x}} = \dot{\mathbf{x}}_0 w = \mathbf{n}(\lambda_m \nu) w, \tag{6}$$

with

$$\nu = \frac{k_B T m_0}{\Omega \lambda_m},$$

where ν can be regarded as the eigenfrequency of the chosen grid which is characterized by the used scaling length λ_m. m_0 is the pre-exponential factor of the mobility.

§ 6. Normalization of the switching probabilities

The eigenfrequency ν given in equation (6) represents the basic attack frequency for *one* particular grain boundary with a constant mobility. However, in order to use a wider spectrum of mobilities and driving forces in one simulation it is necessary to normalize equation (6) by a common grid attack frequency ν_0:

$$\dot{\mathbf{x}} = \dot{\mathbf{x}}_0 w = \mathbf{n}\lambda_m \nu_0 \left(\frac{\nu}{\nu_0}\right) w = \hat{\dot{\mathbf{x}}}_0 \left(\frac{\nu}{\nu_0}\right) w = \hat{\dot{\mathbf{x}}}_0 \hat{w}, \tag{7}$$

where

$$\hat{w} = \frac{\nu}{\nu_0} \frac{p\Omega}{k_B T} \exp\left(-\frac{Q_{gb}}{k_B T}\right) = \frac{m_0 p}{\lambda_m \nu_0} \exp\left(-\frac{Q_{gb}}{k_B T}\right). \tag{8}$$

While $\hat{\dot{\mathbf{x}}}$ is determined by the grid size and the grid attack frequency, $\hat{w}$ is determined by the temperature and the experimental input data (see next section).

An appropriate condition for deriving the value of the normalization or grid attack frequency ν_0 can be identified by some straightforward statistical considerations. It is physically plausible that the maximum occurring probability $\hat{w}^{max}$ in one integration step, can never be larger than one, that is

$$\hat{w}^{max} \leqslant \frac{m_0^{max} p^{max}}{\lambda_m \nu_0^{min}} \exp\left(-\frac{Q_{gb}^{min}}{k_B T}\right) \leqslant 1 \tag{9}$$

where m_0^{max} is the maximum occurring pre-exponential factor of the mobility, p^{max} the maximum occurring driving force, ν_0^{min} the minimum allowed grid attack frequency and Q_{gb}^{min} the minimum occurring activation energy. Inserting $\hat{w}^{max} = 1$ into equation (9) allows one to express the normalization frequency as a function of the upper bound input data†.

† The minimum occurring activation energy Q_{gb}^{min} must also be regarded as an upper bound value, since it represents the fastest-growing boundary.

§ 7. The switching decision—renormalization of the grid attack frequency and evaluation of the switching probability by Monte Carlo integration

The transformation rule derived from the linearized symmetric Turnbull equation defines the normalized switching probability of each grid point as a function of its previous state and the state of the neighbouring grid points (equations (7) and (8)). This section shows how the local switching probability is calculated and how the actual decision about a switching event is for each grid point made using a weighted random sampling Monte Carlo step.

The statistics associated with Monte Carlo integrations make it necessary to re-evaluate equation (9) for the derivation of the value of the normalization frequency ν_0. The statistical variance σ associated with random sampling integration is proportional to $1/N^{1/2}$, where N is the number of trials. The probabilistic constraint for the normalization frequency expressed by equation (9) can for the Monte Carlo integration therefore be increased by the statistical condition that the maximum possible switching probability $\hat{w}^{\max}$ should not only be equal to or smaller than one (equation (9)), but

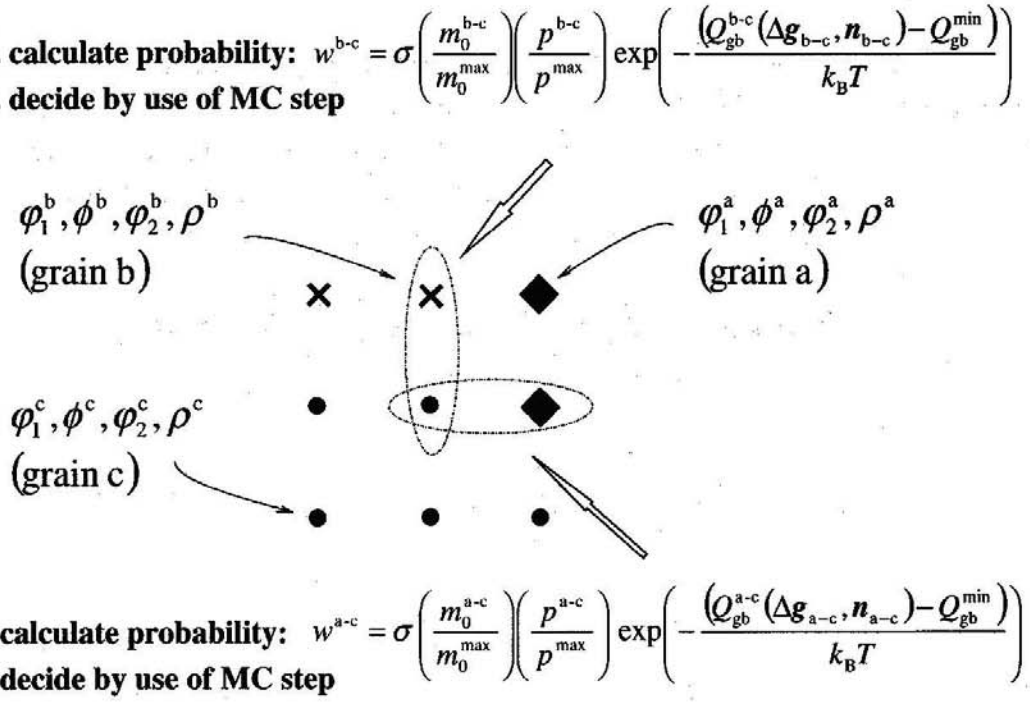

Figure 3. According to equations (4) and (11), non-vanishing switching probabilities occur for lattice cells which reveal neighbouring cells with a misorientation larger than 15° (defining a mobile grain boundary between them) and a driving force which points in their direction. The figure shows a cell of grain c (symbolized by a full circle) which can be switched by its neighbour cell in grain b (symbolized by a cross) or by its neighbour cell in grain a (symbolized by a rotated full square). For simplicity, only nearest neighbours are considered in this diagram. The simulation proceeds by calculating the switching probability of cell c due to cell b according to equation (11), $w_{b-c} = [(m_0^{b-c} p^{b-c})/(m_0^{\max} p^{\max})]\sigma \exp[-(Q_{gb}^{b-c} - Q_{gb}^{\min})/k_B T]$, and the switching probability of cell c due to cell a, $w_{a-c} = [(m_0^{a-c} p^{a-c})/(m_0^{\max} p^{\max})]\sigma \exp[-(Q_{gb}^{a-c} - Q_{gb}^{\min})/k_B T]$, where m_0^{a-c} and m_0^{b-c} are the pre-exponential factors of the grain-boundary mobilities between the two pairs of cells, p^{a-c} and p^{b-c} the local driving forces between them, Q_{gb}^{a-c} and Q_{gb}^{b-c} the activation energies of the grain boundary mobilities, $m_0^{\max}$ the maximum occurring pre-exponential factor of the grain boundary mobility, $p^{\max}$ the maximum occurring driving force and $Q_{gb}^{\min}$ the minimum occurring activation energy of grain boundary mobility. After calculating the switching probability for each pair the actual decision about a switch is made using a Monte Carlo step.

that it should even be smaller than some maximum allowed statistical variance σ, that is $\hat{w}^{\max} \leqslant \sigma$. The appropriate normalization frequency for a set of given parameters and a prescribed maximum statistical error can therefore be calculated according to

$$\nu_0^{\min} \geqslant \frac{m_0^{\max} p^{\max}}{\lambda_m \sigma} \exp\left(-\frac{Q_{gb}^{\min}}{k_B T}\right). \tag{10}$$

Equation (10) modifies the original expression for the local switching probability $\hat{w}^{\text{local}}$ as introduced in equation (8) into

$$\hat{w}^{\text{local}} = \frac{m_0^{\text{local}} p^{\text{local}}}{\lambda_m \nu_0} \exp\left(-\frac{Q_{gb}^{\text{local}}}{k_B T}\right) = \sigma \frac{m_0^{\text{local}}}{m_0^{\max}} \frac{p^{\text{local}}}{p^{\max}} \exp\left(-\frac{Q_{gb}^{\text{local}} - Q_{gb}^{\min}}{k_B T}\right) \tag{11}$$

using $\nu_0^{\min}$ as the grid attack frequency (equation (10)) (figure 3). Equation (11) is the central transformation equation of the method. It shows that the local switching probability can for each grid point be easily expressed in terms of the local mobility m^{local}, which depends on the local misorientation, the local driving pressure p^{local} and the maximum allowed statistical variance σ. The probability of the fastest occurring boundary segment (characterized by $m_0^{\text{local}} = m_0^{\max}$, $p^{\text{local}} = p^{\max}$ and $Q_{gb}^{\text{local}} = Q_{gb}^{\min}$) to realize a local transformation amounts to σ. The characteristic time constant of the simulation Δt is $1/\nu_0^{\min}$.

The simulation proceeds by switching all cells according to their proper statistical weight, that is by evaluating the individual local switching probabilities $\hat{w}^{\text{local}}$ using the Monte Carlo algorithm. This means that for each grid point the calculated transformation or switching probability (equation (11)) is compared with a randomly generated number which lies between zero and unity. The switch is accepted if the random number is equal to or smaller than the calculated transformation probability. Otherwise the switch is rejected.

Figure 4 shows the linear relation between the time constant of the simulation and the statistical variance of the Monte Carlo integration method. All successful

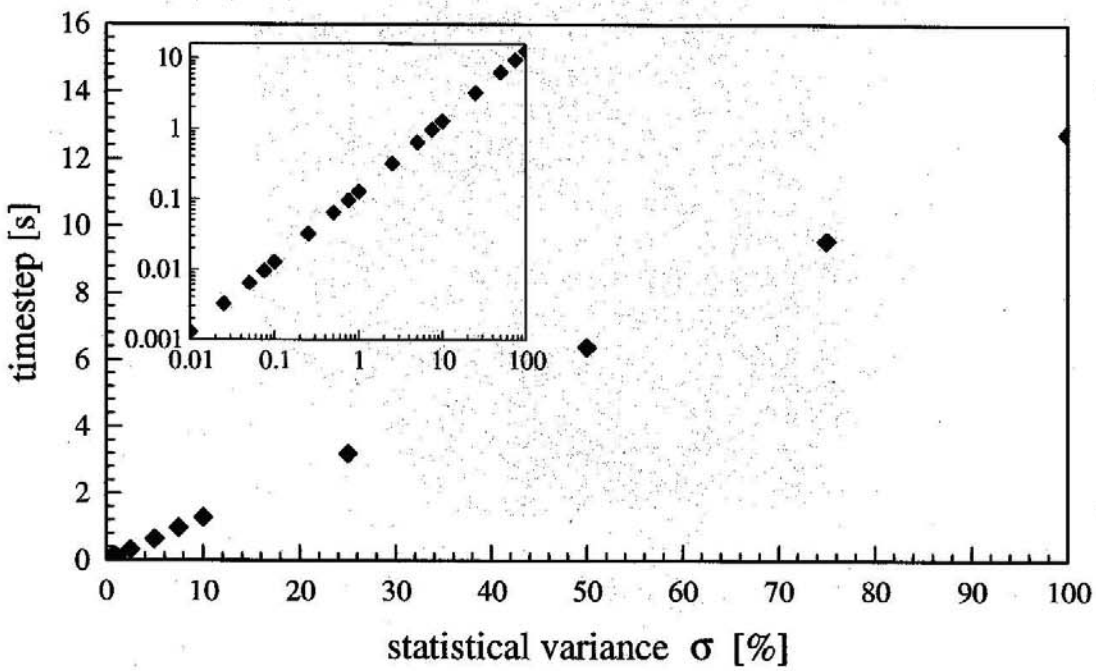

Figure 4. Linear relation between the time constant Δt of the simulation and the statistical variance σ of the Monte Carlo integration method according to equation (10). The characteristic time scale Δt of the simulation is $1/\nu_0^{\min}$. The inset shows the linear relation for small time steps.

cell transformations are updated synchronously once per time interval Δt. Except for the probabilistic evaluation of the single transformation steps, the approach is entirely deterministic.

§ 8. Application of the method to the simulation of primary static recrystallization

Figures 5 (*a*), (*b*) and (*c*) show simulated 3D microstructures of a recrystallizing aluminum single crystal after 0.71 s and 32.2 vol.% recrystallized, after 1.41 s and 78.1 vol.% recrystallized, and after 2.11 s and 99.9 vol.% recrystallized respectively. The initial deformed single crystal had a uniform Goss orientation (011)[100] and a dislocation density of $10^{15}\,\mathrm{m}^{-2}$. The driving force was due to the stored elastic energy. The recovery and driving forces arising from local boundary curvature were not considered. The simulation used site-saturated nucleation conditions, that is the nuclei were at $t = 0\,\mathrm{s}$ statistically distributed in physical space and orientation space. Euler space was discretized into a set of 936 single texture components. The grid size was $10\,\mu\mathrm{m} \times 10\,\mu\mathrm{m} \times 10\,\mu\mathrm{m}$. The cell size was 0.1 μm. All grain boundaries had the same mobility. The activation energy of the grain boundary mobility was 1.3 eV. The pre-exponential factor of the boundary mobility was $m_0 = 6.2 \times 10^{-6}\,\mathrm{m}^3\,\mathrm{N}^{-1}\,\mathrm{s}^{-1}$. The temperature was 800 K. The time constant of the simulation was 0.35 s. The experimental grain-boundary data were taken from the work of Shvindlerman *et al.* (1995), Gottstein *et al.* (1997) and Molodov *et al.* (1998). The Avrami and the Cahn–Hagel plots are given in figure 6.

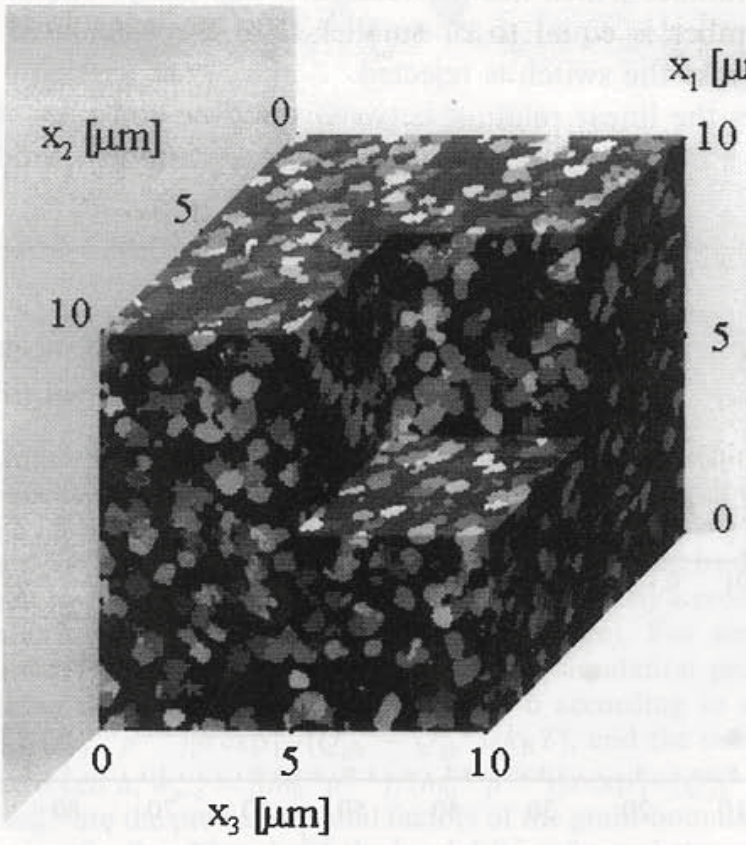

(*a*)

Figure 5. Simulated microstructures of a recystallizing aluminium single crystal: (*a*) 0.71 s, 32.2 vol.% recrystallized volume fraction; (*b*) 1.41 s, 78.1 vol.% recrystallized volume fraction; (*c*) 2.11 s, 99.9 vol.% recrystallized volume fraction.

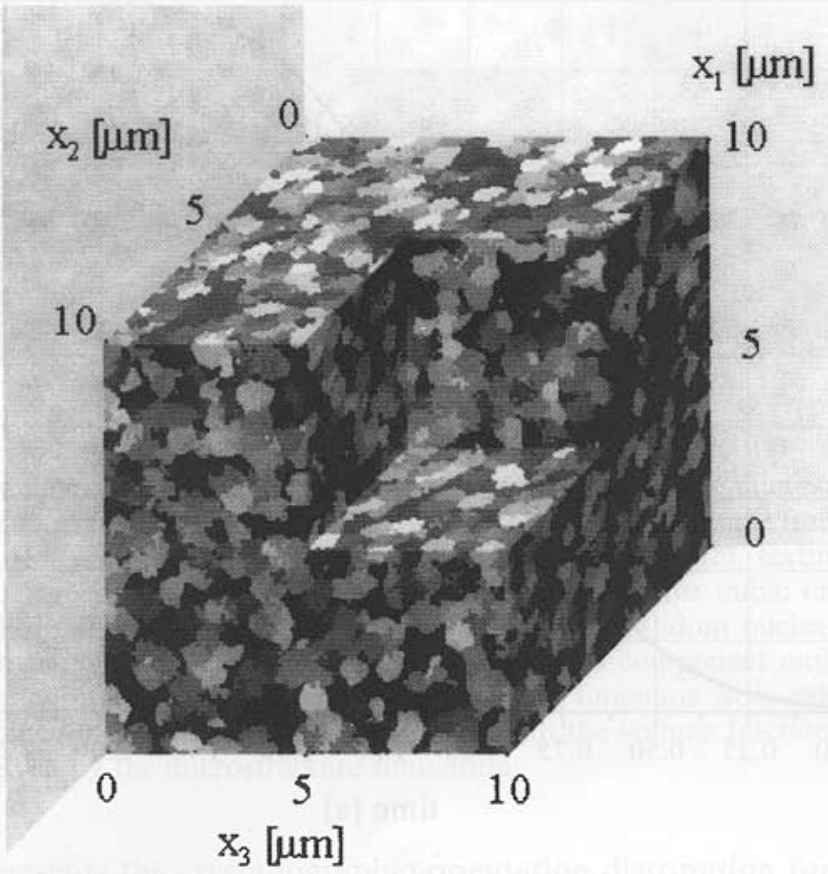

(*b*)

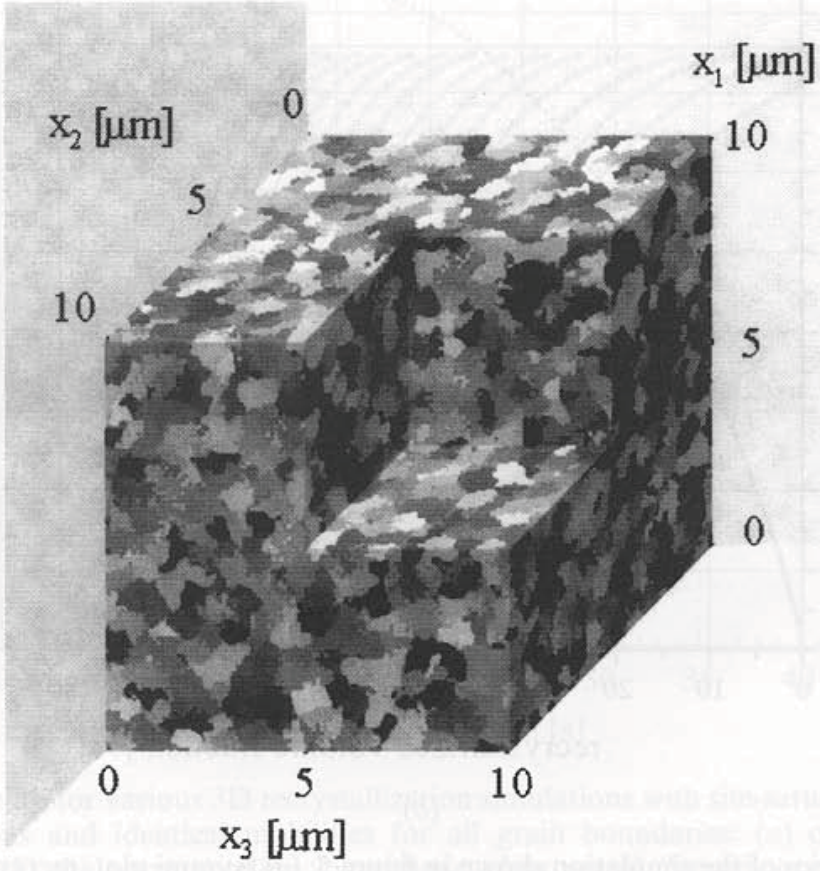

(*c*)

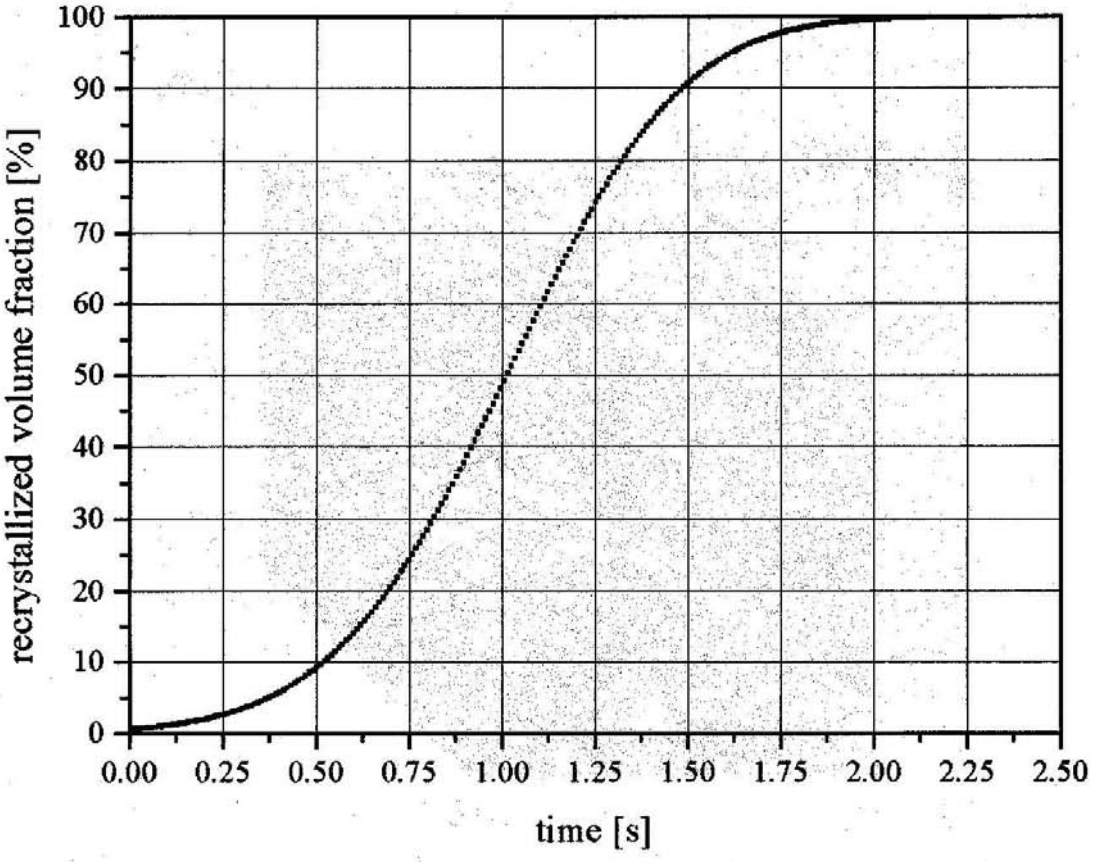

(*a*)

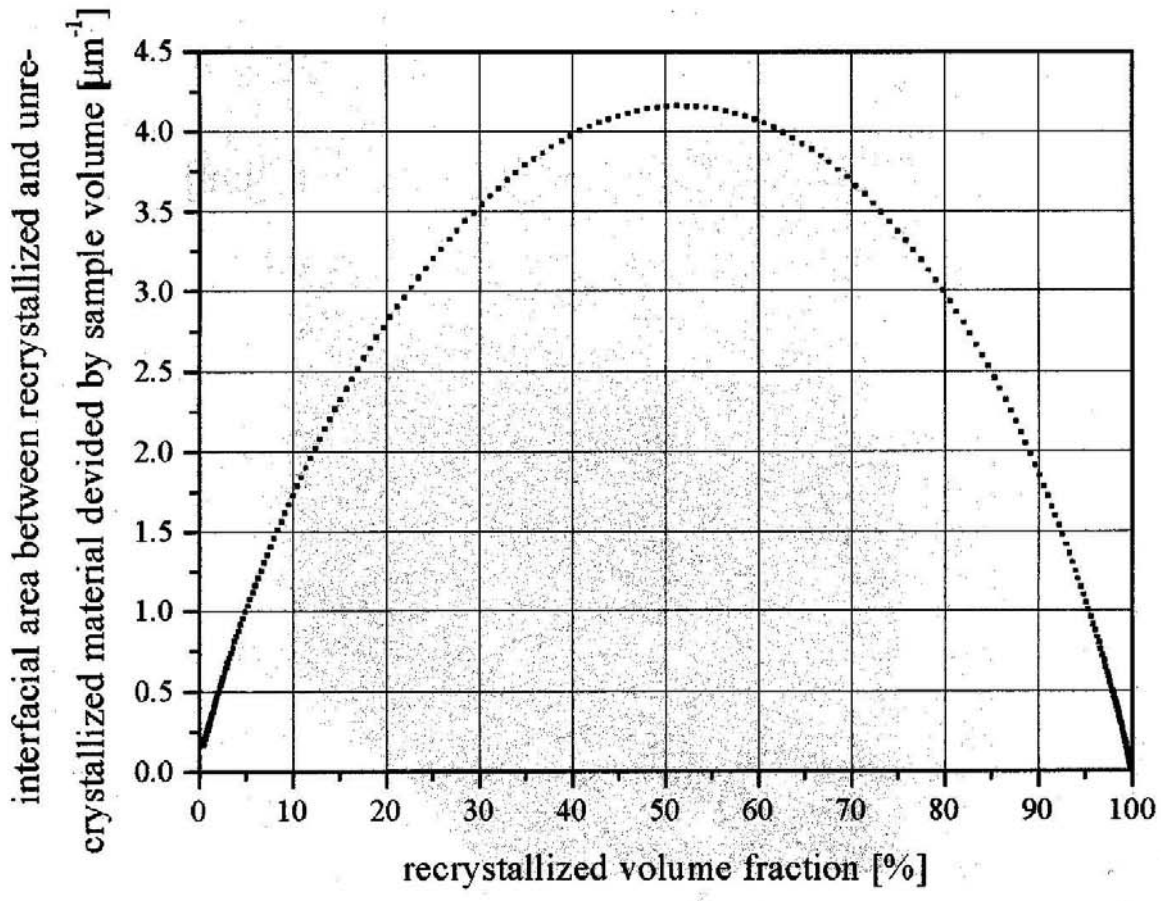

(*b*)

Figure 6. Kinetics of the simulation shown in figure 5: (*a*) Avrami plot, recrystallized volume fraction as a function of the annealing time; (*b*) Cahn–Hagel plot, interfacial area between recrystallized and non-recrystallized material divided by the sample volume.

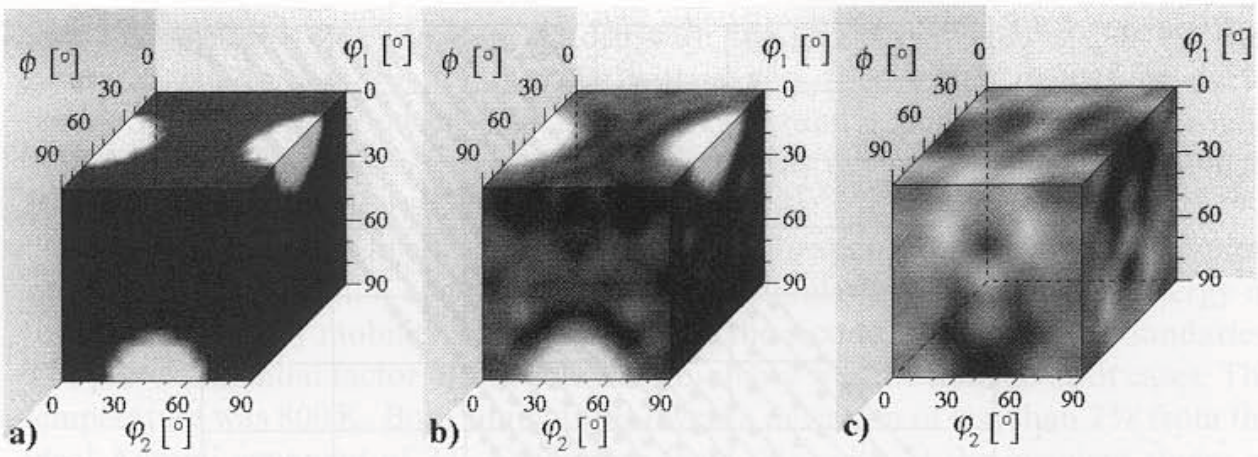

Figure 7. Crystallographic orientation distribution functions for the microstructures shown in figure 5: (*a*) texture after 0.71 s, 32.2 vol.% recrystallized volume fraction; (*b*) texture after 1.41 s, 78.1 vol.% recrystallized volume fraction; (*c*) texture after 2.11 s, 99.9 vol.% recrystallized volume fraction. Euler space for cubic crystal symmetry and orthorhombic sample symmetry. Because of the random nucleation texture the initial strong Goss orientation remains the dominant component until the late stages of recrystallization. The orientation distribution functions were calculated using a Gauss function for each texture component with the volume fractions and the Euler angles given by the microstructure simulation.

Figure 7 presents the crystallographic orientation distribution functions for the three microstructures shown in figure 5. Since the nuclei were randomly distributed in orientation space and no special boundaries were considered, the initial Goss texture remains the dominant component within a nearly random texture until the late stages of recrystallization. The orientation distribution functions were calculated

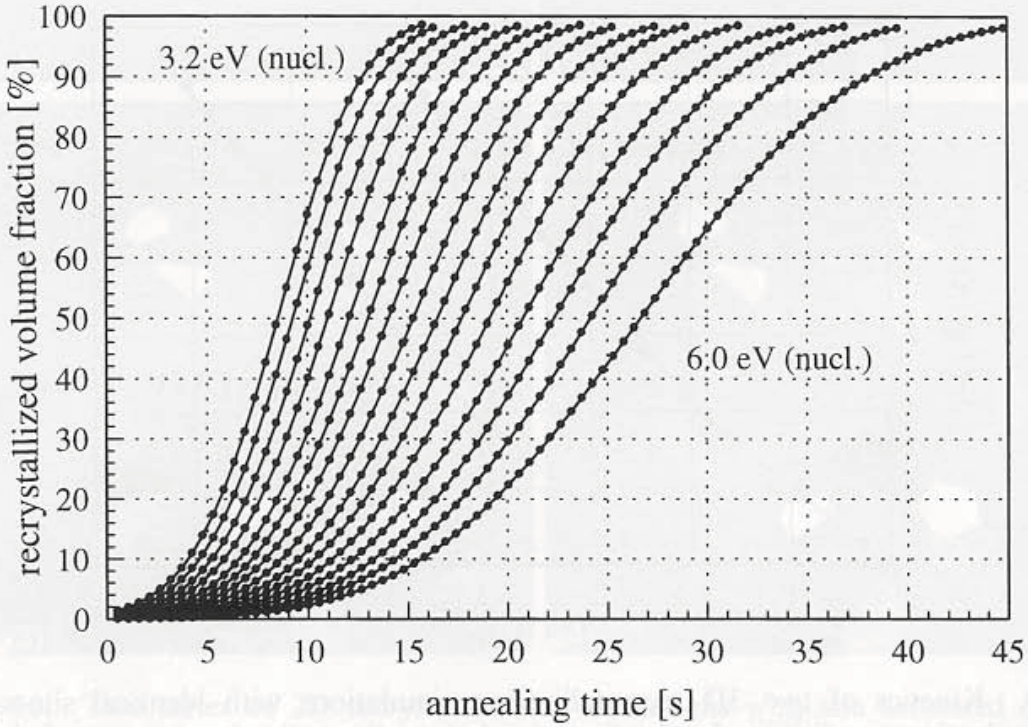

Figure 8. Kinetics for various 3D recrystallization simulations with site-saturated nucleation conditions and identical mobilities for all grain boundaries: (*a*) classical Avrami curves; (*b*) the corresponding logarithmic plots reveal Avrami exponents between 2.86 and 3.13 which is in very good accord with the analytical value of 3.0 for site-saturated conditions.

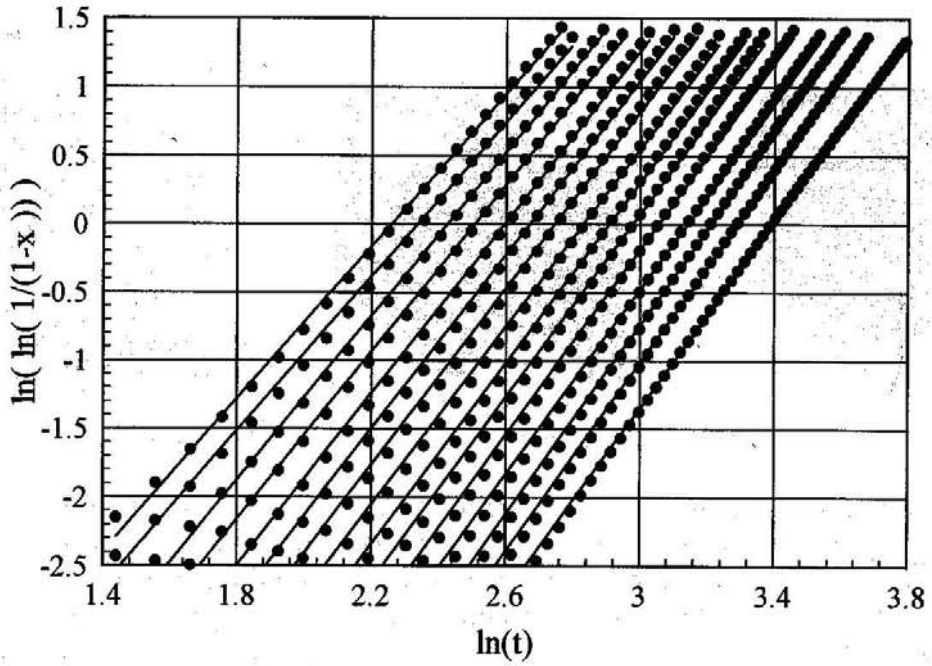

(*b*)

Figure 8.

by using a Gauss function for each texture component with the volume fractions and the Euler angles given by the microstructure simulation.

Figure 8 shows the kinetics for a number of 3D recrystallization simulations with site-saturated nucleation conditions and identical mobilities for all grain boundaries. The different curves correspond to different initial numbers of nuclei. The number of nuclei varied between 9624 (pseudonucleation energy 3.2 eV) and 165 (pseudo-nucleation energy 6.0 eV). The Avrami curves (figure 8 (*a*)) all show a very classical shape and the logarithmic plots (figure 8 (*b*)) reveal Avrami exponents between 2.86

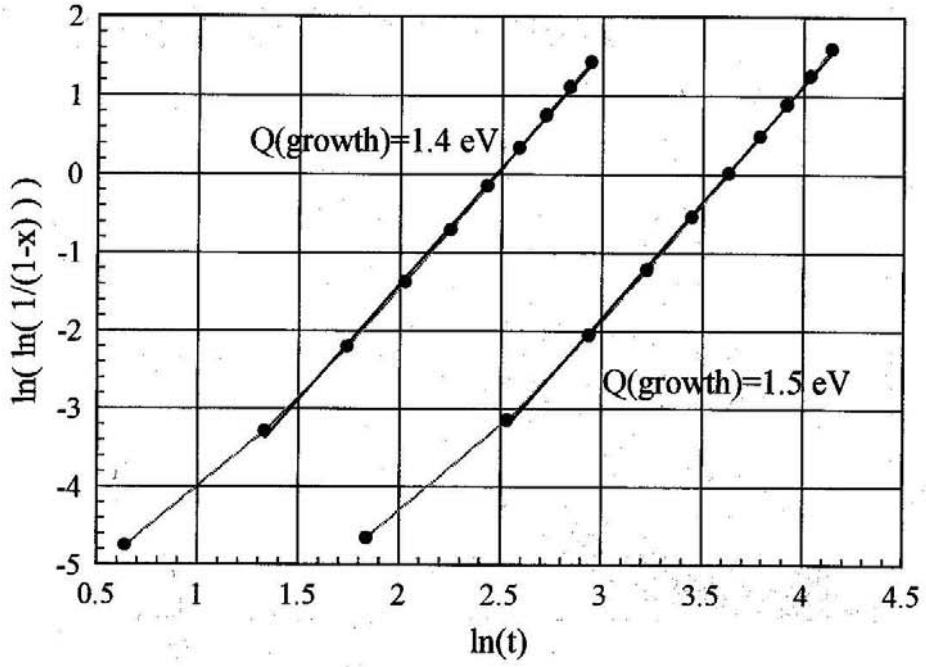

Figure 9. Kinetics of two 3D recrystallization simulations with identical site-saturated nucleation conditions. In the first simulation, the activation energy of the grain-boundary mobility was 1.4 eV and, in the second, 1.5 eV for all boundaries. The pre-exponential factors of the boundary mobility were the same in both cases. The temperature was 800 K. Both simulations reveal a deviation of less than 2% from the ideal Avrami exponent of 3.0. Deviations from this value at the incipient stages of the simulations are attributed to grid effects.

and 3.13 which is in very good accord with the analytical value of 3.0 for site-saturated conditions. The simulations with a very high initial density of nuclei revealed a more pronounced deviation of the Avrami exponent to values around 2.7 in the incipient stages of recrystallization. This deviation from the analytical behaviour can be attributed to grid effects.

Figure 9 shows the kinetics of two 3D recrystallization simulations with identical site-saturated nucleation conditions. In the first simulation the activation energy of the grain boundary mobility was 1.4 eV and, in the second, 1.5 eV for all boundaries. The pre-exponential factor of the boundary mobility was the same in both cases. The temperature was 800 K. Both simulations reveal a deviation of less than 2% from the ideal Avrami exponent of 3.0. Deviations from this value at the incipient stages of the simulations are attributed to grid effects.

Figure 10 shows two series of two-dimensional (2D) recrystallization simulations with site saturated nucleation conditions. The first simulation (figure 10 (*a*))

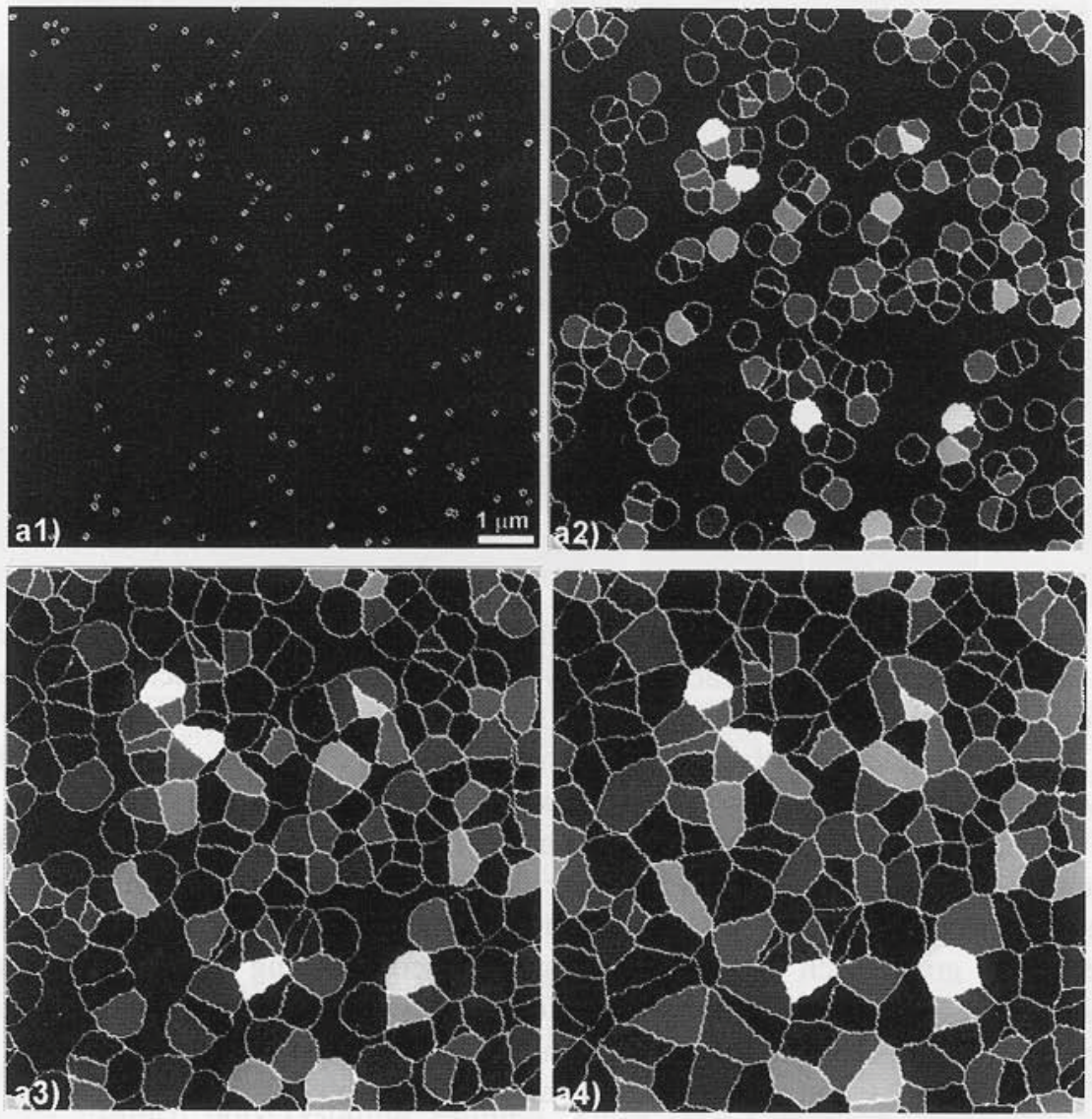

Figure 10. Two series of 2D recrystallization simulations with site saturated nucleation conditions. (*a*) Simulation with identical mobilities for all grain boundaries: (*a*1) 3% recrystallized; (*a*2) 22% recrystallized; (*a*3) 69% recrystallized; (*a*4) 94% recrystallized. (*b*) Simulation using three different types of grain boundary, characterized by different values of the activation energy of the grain-boundary mobility, namely 1.40 eV, 1.45 eV, and 1.50 eV: (*b*1) 1% recrystallized; (*b*2) 17% recrystallized; (*b*3) 62% recrystallized; (*b*4) 92% recrystallized.

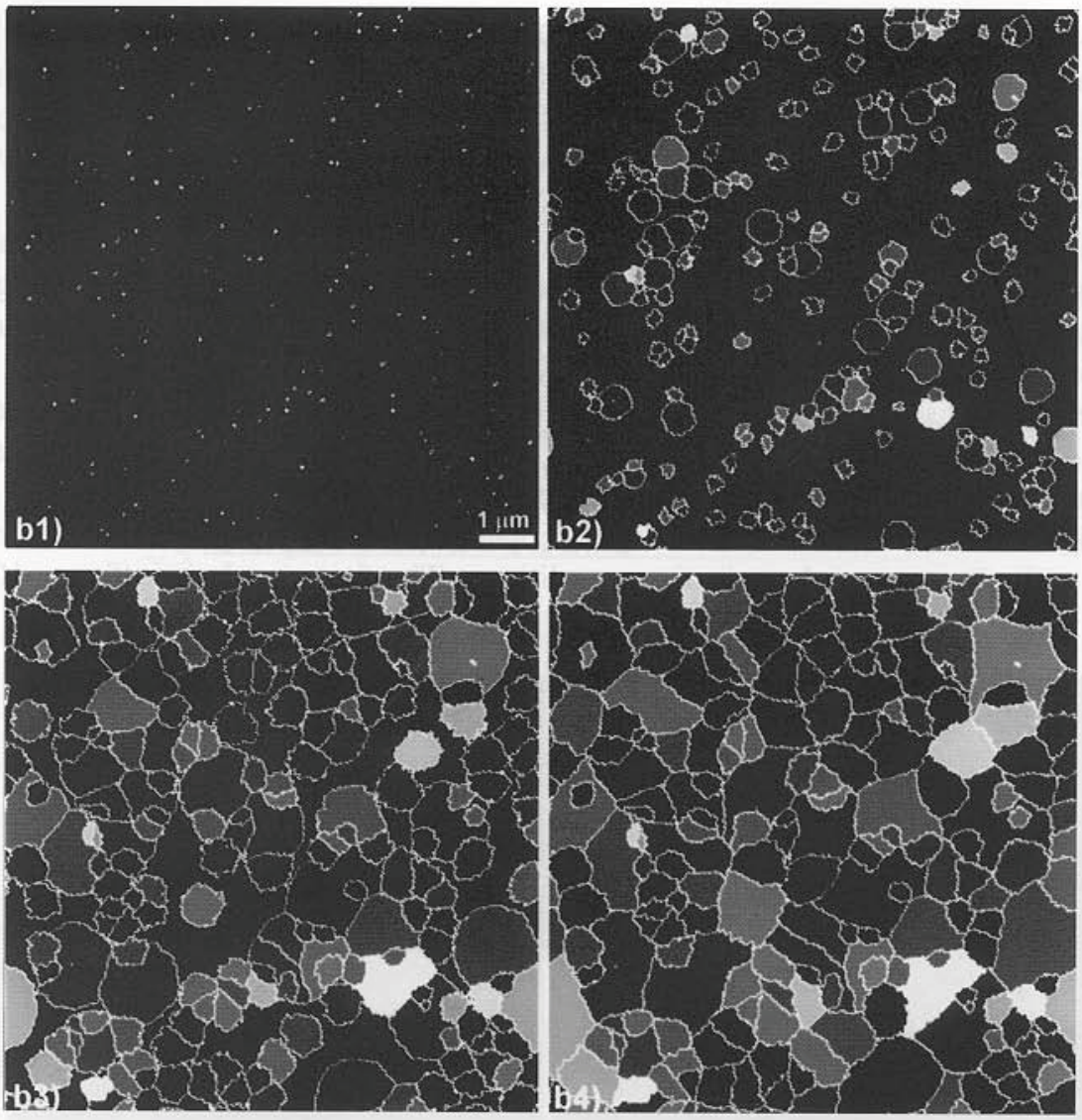

Figure 10.

assumed identical mobility for all grain boundaries which leads to the classical Voronoi† morphology. The second simulation (figure 10 (*b*)) used three different types of grain-boundary, characterized by different values of the activation energy of the grain-boundary mobility, namely 1.40, 1.45 and 1.50 eV. A comparison of both microstructures clearly shows the influence of the heterogeneity of grain-boundary mobility on the final grain topology.

Figure 11 shows the effect of grain-boundary mobility on growth selection. While in figure 11 (*a*) all boundaries had the same mobilities, in figure 11 (*b*) one grain had a higher mobility than the others (activation energy of 1.35 eV instead of 1.40 eV) and consequently grew much more rapidly than the neighbouring grains, which finally ceased to grow. The grains in this simulation all grew into a heavily deformed single crystal. The influence of boundary curvature was not considered.

Figure 12 shows two subsequent 2D simulation sketches of recrystallizing aluminium. The upper figures depict the orientation images, that is each grey level represents a different crystal orientation. The lower figures show the corresponding stored dislocation densities. The white areas are recrystallized, that is their stored dislocation content was dropped to zero. The predictions were obtained by applying the probabilistic cellular automaton algorithm to crystal plasticity finite element

† A Voronoi structure is a Wigner–Seitz construction applied to a random array of points.

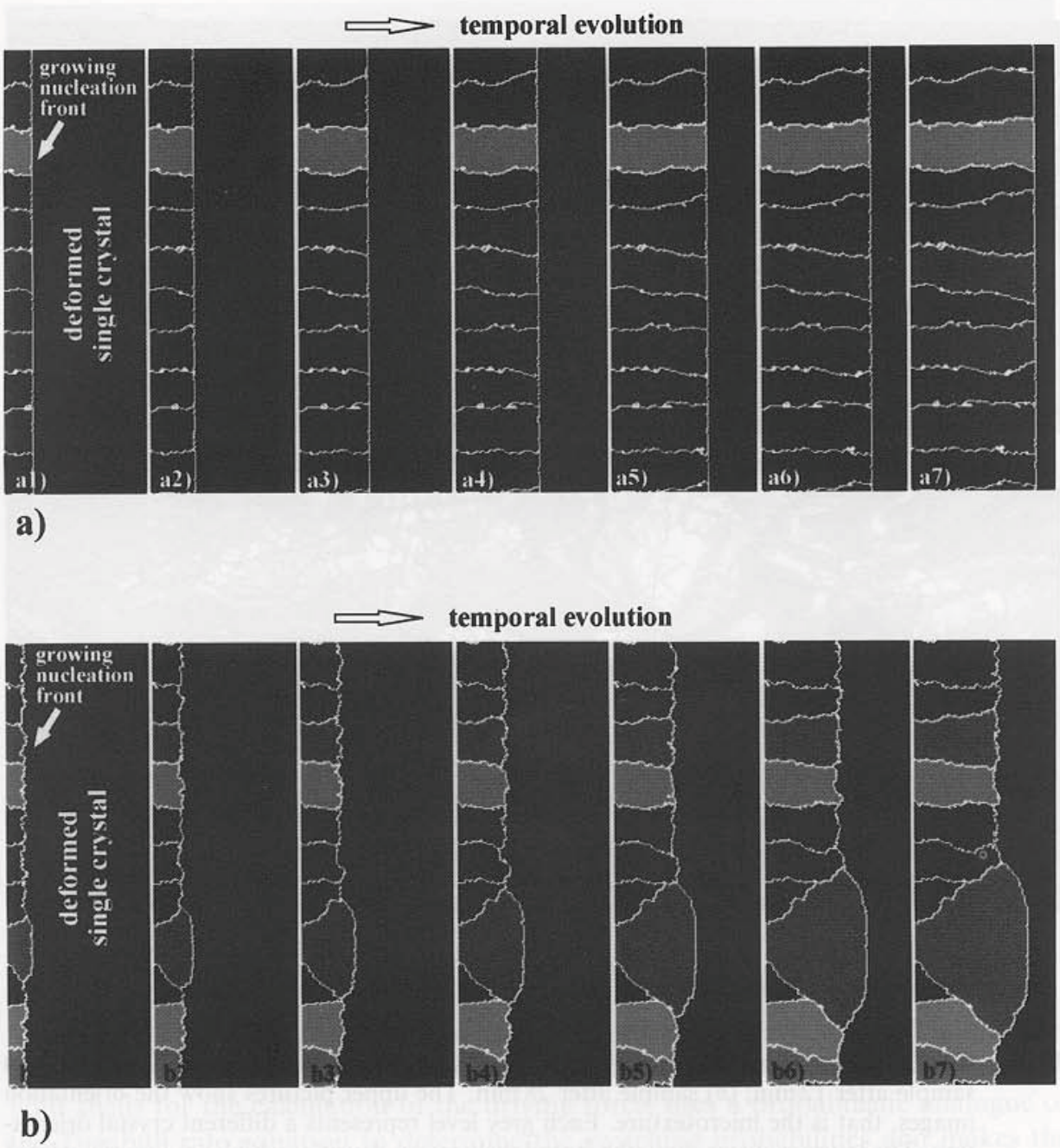

Figure 11. 2D recrystallization simulations which demonstrate the effect of grain-boundary mobility on growth selection (all nuclei in this simulation grew into a heavily deformed single crystal): (*a*) All boundaries had the same mobility. The figure shows seven subsequent stages of growth, indicated by (*a*1)–(*a*7). (*b*) One grain had a higher mobility than the others and grew much more rapidly than the neighbouring grains. The figure shows seven subsequent stages of growth, indicated by (*b*1)–(*b*7).

starting data (Raabe and Becker 1999). The combination of these methods enables one to investigate the influence of local grain-boundary characteristics, local driving forces, and local textures on the formation of microstructure and texture in heterogeneously strained polycrystalline samples. Those cells exhibiting the largest local orientation gradients with respect to their neighbour cells and the largest accumulated local shears were used as recrystallization nuclei. The predictions show that recrystallization in a sample with spatially heterogeneous properties can lead to substantial deviations from the Avrami kinetics, to grain clustering, and to partial recovery of grains which have low driving forces, insufficient misorientations with respect to the growing nuclei, or insufficient nucleation rates.

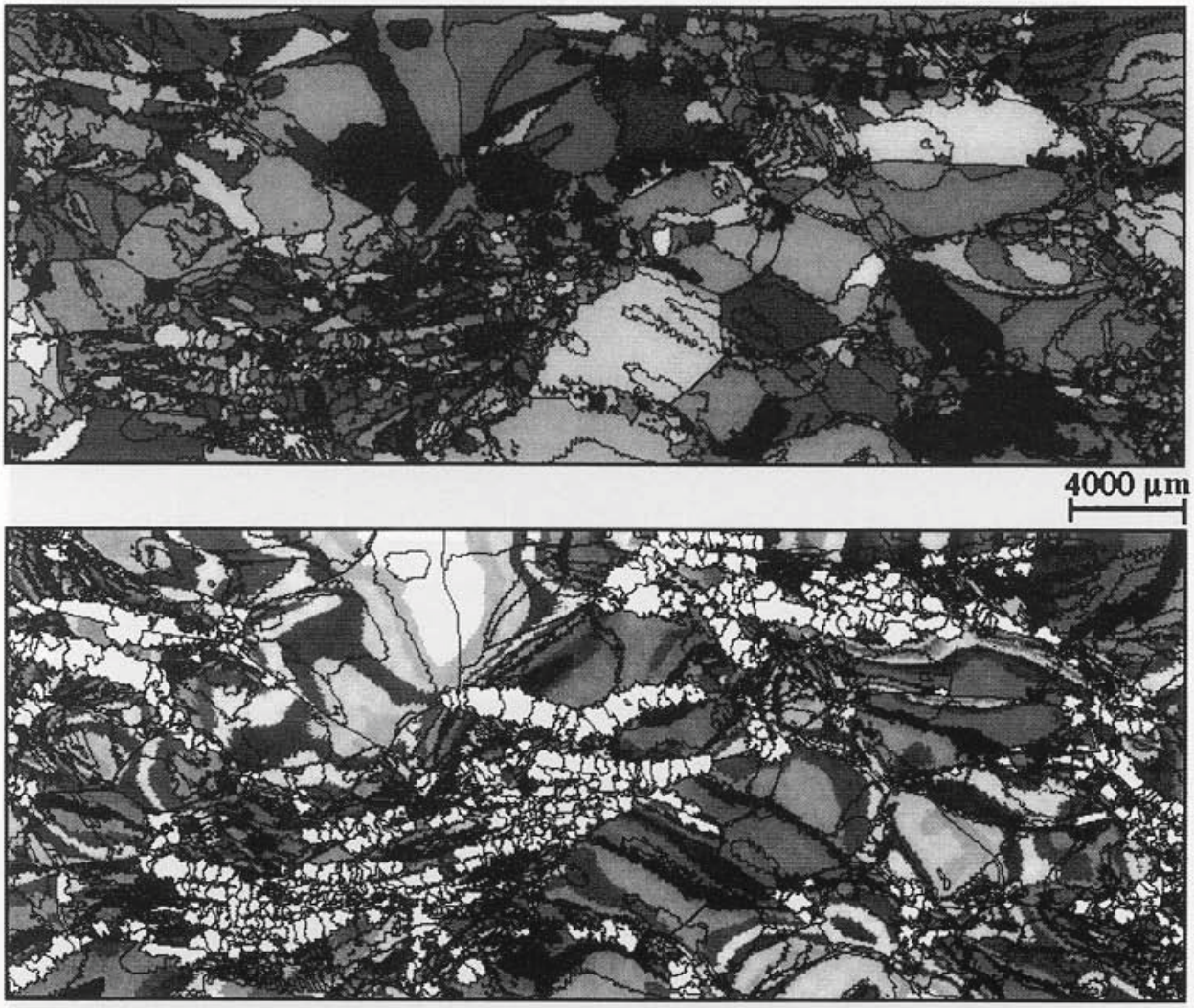

(*a*)

Figure 12. 2D simulations of primary static recrystallization in deformed aluminium: (*a*) sample after 12 min; (*b*) sample after 28 min. The upper pictures show the orientation images, that is the microtexture. Each grey level represents a different crystal orientation. The lower pictures show the stored dislocation densities which are linearly related to the local values of the accumulated shear. The white areas are recrystallized, that is their stored dislocation content was dropped to zero. The predictions were made by applying the probabilistic cellular automaton algorithm to crystal plasticity finite element starting data (Raabe and Becker 1999). Those cells exhibiting the largest local orientation gradients with respect to their neighbour cells and the largest accumulated local shears served as nuclei. The simulation parameters were as follows: cell size, 61.9 µm; activation energy of grain-boundary mobility: 1.46 eV for all grain boundaries; pre-exponential factor of the grain-boundary mobility $m_0 = 6.2 \times 10^{-6}\,\mathrm{m^3\,N^{-1}\,s^{-1}}$; temperature, 800 K; time constant, 2.58 s.

§9. Conclusions

This paper introduced a kinetic cellular automaton method with a probabilistic switching rule for the spatial and crystallographic prediction of mesoscale transformation phenomena that involve orientational field variables and the motion of sharp interfaces. The method is designed to combine the computational simplicity and scalability of a switching model with the physical stringency of a boundary dynamics model. The main results and conclusions are as follows.

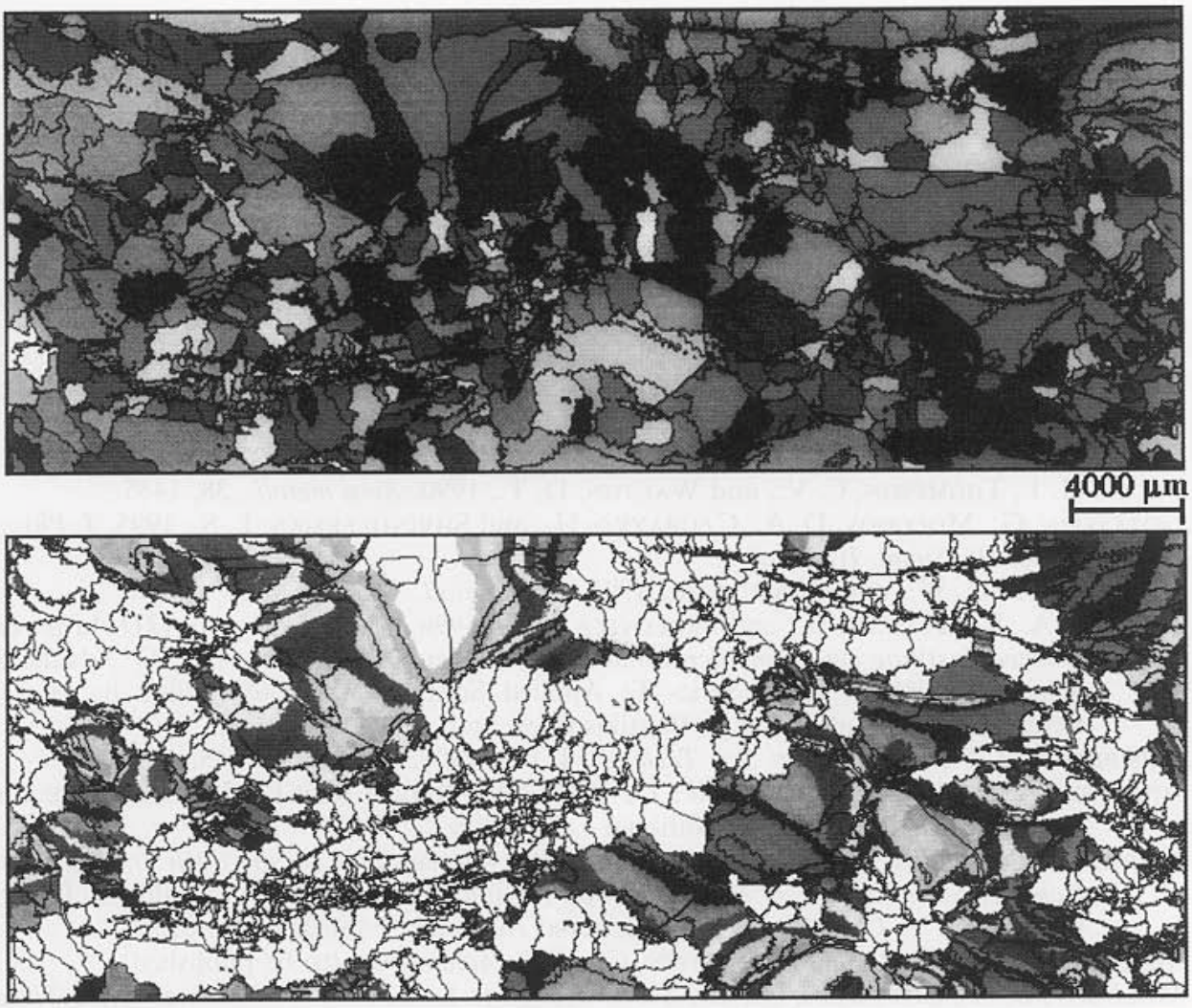

(*b*)

Basic method. The automaton is discrete in time, physical space and orientation space, works on a regular 3D cubic lattice using the first-, second- and third-neighbour shells for the calculation of the driving force, uses a probabilistic analogue of the Turnbull rate equation to determine the switching probabilities and makes the actual switching decision by use of a Monte Carlo step. The transformation rule which is scaled by the local grain boundary mobility, the local crystallographic texture and the local driving force is scalable to any mesh size and to any set of boundary mobility and energy data. The state update of all grid points is made in synchrony.

Application. The method was used for 2D and 3D recrystallization simulations. It properly reproduced typical microstructures, textures and Avrami kinetics which were in very good accord with analytical predictions. Furthermore, the method was combined with crystal plasticity finite element data to simulate recrystallization in a heterogeneously strained material.

Acknowledgements

The author gratefully acknowledges the financial support by the Deutsche Forschungsgemeinschaft through the Heisenberg program and the kind support by the Department for Materials Science and Engineering of Carnegie–Mellon

University. The author is grateful to H. Weiland, A. D. Rollett, R. C. Becker, F. Roters and V. Marx for a number of stimulating discussions.

References

ADAMS, B. L., KINDERLEHRER, D., MULLINS, W. W., ROLLETT, A. D., and TA'ASAN, T. S., 1998, *Scripta mater.*, **38**, 531.

ANDERSON, M. P., and ROLLETT, A. D., 1990, *Simulation and Theory of Evolving Microstructures* (New York: Minerals, Metals and Materials Society).

CHEN, L. Q., 1995, *Scripta metall.*, **32**, 115.

FAN, D., GENG, C., and CHEN, L. Q., 1997, *Acta metall.*, **45**, 1115.

FRADKOV, V. E., GLICKSMAN, M. E., PALMER, M., and RAJAN, K., 1994, *Acta metall.*, **42**, 2719.

FROST, H. J., and THOMPSON, C. V., 1987, *Acta metall.*, **35**, 529.

FROST, H. J., THOMPSON, C. V., and WALTON, D. T., 1990, *Acta metall.*, **38**, 1455.

GOTTSTEIN, G., MOLODOV, D. A., CZUBAYKO, U., and SHVINDLERMAN, L. S., 1995, *J. Phys., Paris, IV, Suppl. III*, **5**, c3–9.

HESSELBARTH, H. W., and GÖBEL, I. R., 1991, *Acta metall.*, **39**, 2135.

HOLM, E. A., ROLLETT, A. D., and SROLOVITZ, D. J., 1996, *Proceedings of NATO Advanced Science Institute on Computer Simulation in Materials Science*, NATO Advanced Science Institutes Series, Series E: Applied Sciences, Vol. 308, edited by H. O. Kirchner, L. P. Kubin and V. Pontikis (Deventer: Kluwer), p. 373.

HUMPHREYS, J. F., 1992, *Mater. Sci. Technol.*, **8**, 135; 1997, *Acta metall.*, **45**, 4231.

JUUL JENSEN, D., 1992, *Scripta metall.*, **27**, 1551; 1997, Report Risø-R-978 (EN), Materials Research Department, Risø National Laboratory.

MARX, V., RAABE, D., and GOTTSTEIN, G., 1996, *Proceedings of the 11th International Conference on Textures of Materials*, Vol. 1, Xian, September 1996, edited by Z. Liang, L. Zuo and Y. Chu (Beijing: International Academic Publishers), p. 515.

MARX, V., REHER, F. R., and GOTTSTEIN, G., 1998, *Acta mater.* (to be published).

MOLODOV, D. A., GOTTSTEIN, G., and SHVINDLERMAN, L. S., 1998, *Proceedings of the Third International Conference on Grain Growth*, Carnegie–Mellon University, Pittsburgh, Pennsylvania, June 1998 (to be published).

PEZZEE, C. E., and DUNAND, D. C., 1994, *Acta metall.*, **42**, 1509.

RAABE, D., 1998a, *Mater. Sci. Forum*, **273–275**, 169; 1998b, *Proceedings of the Third International Conference on Grain Growth*, Carnegie–Mellon University, Pittsburgh, Pennsylvania, June 1998 (to be published).

RAABE, D., and BECKER, R. C., 1999 (to be published).

SHVINDLERMAN, L. S., CZUBAYKO, U., GOTTSTEIN, G., and MOLODOV, D. A., 1995, *Microstructural and Crystallographic Aspects of Recrystallization*, Proceedings of the 16th Risø International Symposium on Materials Science: edited by N. Hansen, D. Juul Jensen, Y. L. Liu and B. Ralph (Risø, Roskilde: Risø National Laboratory), p. 545.

SROLOVITZ, D. J., 1986, *Computer Simulation of Microstructural Evolution* (Warrendale, Pennsylvania: Metallurgical Society of AIME).

SVOBODA, J., 1996, *Scripta metall.*, **28**, 1589.

TURNBULL, D., 1951, *Trans. AIME*, **191**, 661.